Dispersion in the SERS Enhancement with Silver Nanocube Dimers

Seung Yong Lee,[†] Ling Hung,[‡] Garrett S. Lang,[‡] Jane E. Cornett,[†] Isaak D. Mayergoyz,[‡,§] and Oded Rabin[†,§,*]

[†]Department of Materials Science and Engineering, [‡]Department of Electrical and Computer Engineering, and [§]Center for Applied Electromagnetics, Institute for Research in Electronics and Applied Physics, University of Maryland, College Park, Maryland 20742, United States

ABSTRACT The SERS phenomenon was studied using a large set of silver nanocube dimers programmed to self-assemble in preset locations of a patterned substrate. This SERS substrate made it possible to demonstrate the dependence of the SERS enhancement on the geometry of the silver nanocube dimers and to quantify the dispersion in the SERS enhancement obtained in an ensemble of dimers. In addition to the effects of the gap distance of the dimer and the orientation of the dimer axis relative to the laser polarization on SERS enhancement, the data reveal an interesting dependence of the site-to-site variations of the enhancement on the relative orientation of the nanocubes in the dimer. We observed the highest heterogeneity in the SERS signal intensity with face-to-face dimers and a more robust SERS enhancement with face-to-edge dimers. Numerical calculations indicate that the plasmon resonance frequencies of face-to-face dimers shift considerably with small changes in gap distance. The resonance frequency shifts make it less likely for many of the dimers to satisfy the matching condition between the photon frequencies and the plasmon resonance frequency, offering an explanation for the large site-to-site variations in SERS signal intensity. These results indicate that plasmonic nanostructure designs for SERS substrates for real-world applications should be selected not only to maximize the signal enhancement potential but also to minimize the heterogeneity of the substrate with respect to signal enhancement. The latter criterion poses new challenges to experimentalists and theorists alike.

KEYWORDS: Raman scattering · nanocube · plasmon · resonance · silver · self-assembly

Surface-enhanced Raman scattering (SERS) is a powerful technique that provides high sensitivity and high specificity for molecular spectroscopy.[1,2] The dominant part of the enhancement in SERS in comparison to normal Raman scattering is thought to originate from the interaction of the incident and scattered photons with plasmon modes in a nanostructured metal surface (known as *the electromagnetic mechanism* of enhancement).[3] A large volume of scientific work has been dedicated to determining the enhancement factor (EF) by which the molecular SERS signal is amplified, as well as clarifying why the EF varies by orders of magnitude from substrate-to-substrate, site-to-site, and target molecule-to-molecule. To date, the single molecule detection capabilities of SERS have been demonstrated,[4−10] but there is no reliable method to fabricate substrates that consistently provide this enhancement. Nevertheless, the understanding of the SERS phenomena is being progressively advanced, in part as a consequence of improvements in nanoscale substrate design.[11] The SERS enhancement has been associated with "hot-spots", locations on the surface of the metal where under resonance conditions near-field field intensities are orders of magnitude larger than the far-field intensity. Hot-spots are easily generated by the aggregation of metal nanoparticles[12,13] (or the placement of a particle over a metallic substrate[14]). The field enhancement depends on the shape of the nanoparticles, on the gap distance between the nanoparticles, and on the curvature of the nanoparticles near the gap.[15,16] Recently, efforts have been dedicated to studying the SERS phenomena in small clusters of nanoparticles of well-defined shapes to elucidate the effect of nanoscale structure on the optical properties. For example, hot-spots were demonstrated and EFs were reported for nanosphere dimers,[17,18] nanoshell dimers,[18] nanocube dimers,[19,20] octahedra dimers,[21] and nanoparticle−nanowire dimers[22,23] carrying adsorbed monolayers of molecules. High-resolution transmission electron microscopy of low-symmetry nanoparticle dimers used for single molecule spectroscopy was also reported.[8] These experiments are often based on randomly generated clusters of preformed nanoparticles that have been drop-casted and are located by scanning over large areas of the substrate using dark-field imaging.[8,13,24] As a result, these studies sampled a very small number of plasmonic structures and commonly reported a single value of EF for a given cluster geometry. Notably, effects of sample heterogeneity cannot be fully addressed using this approach.

*Address correspondence to oded@umd.edu.

Received for review June 30, 2010 and accepted September 28, 2010.

Published online October 7, 2010. 10.1021/nn101484a

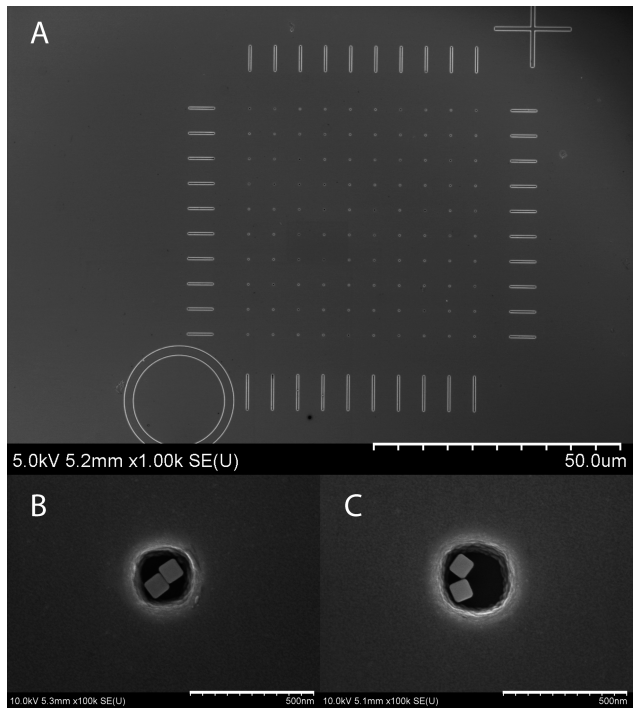

Figure 1. SEM images of (A) the patterned substrate and (B,C) dimers in the pores. The full range of the scale bars is 50 μm, 500 nm, and 500 nm, respectively.

Heterogeneity in engineered SERS substrates—large variations in the EF in structures made by a single process—sets challenging requirements on the resolution of the fabrication tools. It is also of great concern with respect to the implementation of SERS in chemical diagnosis. To guarantee that the detection threshold and the reliability of a SERS-based method for molecular sensing are satisfactory, attributes of SERS substrates such as the maximum enhancement factor, the average enhancement factor, and the site-to-site reproducibility need to be assessed quantitatively and optimized.[25] In this article, we demonstrate the benefits of studying a large collection (>200) of silver nanocube (AgNC) dimers to elucidate the parameters that play a significant role in the enhancement of Raman scattering. The dimers are formed in predetermined locations so that the data collection process is efficient. We do not exclude any nanocube dimer from this study, regardless of the magnitude of their scattering cross sections. We therefore were able to quantify the degree of variability of the EF in seemingly similar AgNC dimers. By investigating how the enhancement factor varies within an ensemble of dimers, the origins of SERS substrate heterogeneity may be better understood and addressed. Numerical calculations of the plasmon resonance frequencies and field enhancements as a function of the structure of the dimer were used to gain insight as to the significance of the resonance condition in our system, and in the experiments reported by Prof. Xia's group. Xia *et al.* have recently reported three EF values from three dimers using SERS experiments with similar AgNC dimers,[26] except that the incident and scattered wavelengths analyzed were different than those chosen by us. Understanding the dependence of the enhancement factor on structural parameters is key to the fabrication of useful SERS substrates and is the focus of this article.

RESULTS AND DISCUSSION

The large number of plasmonic nanoparticle clusters was generated by vertical deposition of AgNCs from a colloidal solution using a planar silicon substrate containing prepatterned arrays of submicrometer quasi-cylindrical cavities on the surface (Figure 1). In the vertical deposition process, a substrate is translated vertically upward with respect to the air/solution interface either by means of a motorized stage or by solvent evaporation.[27,28] As the air/solution interface sweeps across the surface of the substrate, nanoparticles are pushed against topographic steps and selectively deposit at the bottom of the steps.[29] This method of choice is simple and scalable. Other approaches are possible, such as the chemical patterning of the substrate using self-assembled monolayers (SAMs) to spatially control the formation of arrays of clusters of nanospheres.[30] However, our method allows the substrate to be reused, greatly increasing the number of clusters that can be studied with minimal use of e-beam lithography. AgNCs were chosen over other nanostructures because they can be synthesized in large quantities, as monodisperse colloidal suspensions, and in various sizes; because they have sharp corners that can focus electric fields; and because they present a uniform surface—the Ag{001} planes—for molecules to adsorb on, making the calculation of enhancement factors more accurate. Furthermore, the use of nanocubes over nanospheres[28] adds complexity to the clusters formed in the process (*e.g.*, variations in the relative azimuthal angle) and in fact leads to higher enhancement factors.[31] Using the described experimental system, we have obtained SERS data and the corresponding scanning electron microscopy (SEM) images for a large collection of dimers, each slightly different from its neighbors.

Figure 1A shows an SEM image of the patterned substrate before the vertical deposition process, and Figure 1B,C shows dimers of AgNCs (average edge length = 80 nm) that have been formed in the cavities of the ready-to-use SERS substrate. Each cavity is isolated from the others and can be probed individually by the laser beam of the micro-Raman system and by electron microscopy. The AgNCs were coated with a self-assembled monolayer of thiol molecules (4-aminobenzenethiol, 4-ABT) that served as Raman dyes. The Raman spectra were collected using a confocal micro-Raman spectrometer equipped with a 632.8 nm laser source. In the following, the *Raman signal intensity* is quantified as the integrated peak area for the

carbon−sulfur bond stretch of 4-ABT at 1078 cm^{-1}. The *SERS substrate enhancement factor* (SSEF) is as defined by Etchegoin *et al.*[32] and calculated as the Raman signal intensity divided by the number of molecules on the AgNCs and by the Raman signal intensity per molecule measured in the absence of the substrate.

We have analyzed the Raman response from cavities containing exclusively two nanoparticles (*i.e.*, AgNC dimers). Plasmonic coupling in *nanosphere* dimers depends only on the interparticle distance and the relative orientation of the incident light polarization with respect to the dimer axis and has been extensively investigated. In nanocube dimers, additional configuration degrees of freedom are present, namely, the relative orientation of each of the nanocubes with respect to the Poynting vector and the electric field of the incident light (*i.e.*, the azimuthal angles and the polar angles). Unfortunately, most of the configuration space is not easily accessible by drop-casting nanocubes on a planar substrate, a process that is heavily biased to form nanocube clusters in which the faces of the nanocubes lay flat on the surface or face each other. This is not the case for self-assembly within submicrometer cavities as used here. We have observed a sizable portion of dimer clusters in which an edge or a vertex point toward the adjacent cube. As a result, more of the configuration space is probed here compared to previous studies.

The effect of dimer axis orientation and gap distance on SERS is only briefly described here because our results match findings extensively reported previously in the literature.[6,15,33−35] Theoretically, the SERS signal intensity should present a $\cos^2\theta$ dependence on the angle θ between the E-field polarization and the dipole moment associated with the excited plasmon resonance mode. In the case of a symmetric dimer in an isotropic medium, the strongest evanescent field at the surface of the nanoparticles is associated with a plasmon mode with polarization parallel to the dimer axis and field localization in the gap between the two particles. The $\cos^2\theta$ dependence has been confirmed experimentally in individual examples of dimers.[22,36−38] We have found the same overall trend (Figure S1, Supporting Information): Collectively, AgNC dimers with large enhancement factors produce a signal that follows the $\cos^2\theta$ dependence, regardless of the precise details of the configuration of each AgNC dimer. Dimers with small enhancement factors deviate from the rule, as expected when plasmonic coupling between the two AgNCs is ineffective. From the practical point-of-view, we conclude that in *engineered SERS substrates made of dimeric structures* (by lithography or by self-assembly) it is imperative to have all the dimer axes aligned in a single orientation that must be communicated to the end-user. For SERS substrates of the type used in this work, alignment can be achieved by milling cavities of rectangular shape. With respect to the influence of the gap distance in dimers of 80 nm AgNCs, we concluded from the data (a) that gap distances smaller than 10 nm are a necessary (but not sufficient) condition for obtaining SSEFs that are distinctively higher than SSEFs of AgNC monomers, and (b) that within the limits of the imaging resolution in this study (~3 nm), the smaller the gap, the higher the potential SERS enhancement from the structure. These results are in agreement with previous studies on the coupling of localized plasmons and its dependence on interparticle gap distance. In some reports, however, effective coupling was observed across gaps larger than 10 nm with similar sized nanostructures.[39−41]

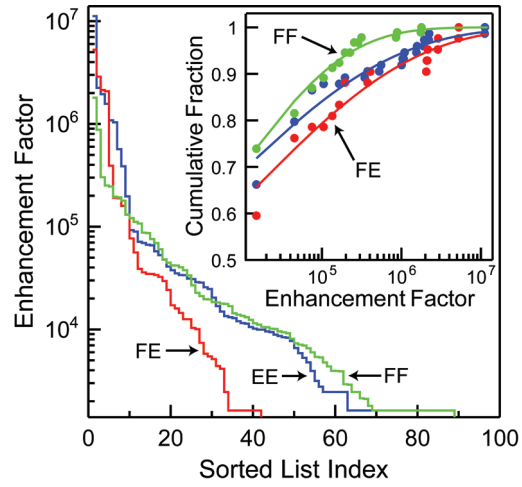

Figure 2. SERS substrate enhancement factors for EE dimers (blue), FE dimers (red), and FF dimers (green). Inset: Experimental cumulative fractions and fit to the Weibull distribution model (solid circles, experimental data; solid lines, fit values; the colors have the same meaning as above).

Investigating the SERS signal dependence on the azimuth (and polar) angles is a more ambitious task because of the large number of possible configurations involved and the relatively weak and poorly understood dependence of the plasmon modes of the dimer on these parameters. We present here a comprehensive analysis of the azimuthal orientation parameter in SERS, utilizing both experimental data from our AgNC clusters and theoretical modeling. Because we anticipate the dependence on azimuth angles to be weaker than the dependence on the dimer axis orientation and the gap distance, a large data set was used (>200 dimers) in conjugation with a statistical analysis model and numerical calculations.

In this analysis, the dimers with gap size smaller than 10 nm were analyzed in three groups: (1) edge-to-edge dimers (EE, 74 dimers); (2) face-to-edge dimers (FE, 42 dimers); and (3) face-to-face dimers (FF, 92 dimers).[42] The SSEFs from each group were arranged in a diminishing sorted list (Figure 2). For each list, we have calculated the cumulative distribution function $F(x)$, indicating the fraction of dimers that give

TABLE 1. Parameters Obtained from the Weibull Distribution Model

	EE dimers	FE dimers	FF dimers
shape parameter	0.196 ± 0.014	0.205 ± 0.017	0.284 ± 0.021
scale parameter	4483 ± 613	10812 ± 1510	5237 ± 683

a SSEF less than or equal to x. Thus $F(x)$ is a monotonic increasing function satisfying: $\lim_{x\to 0}F(x) = 0$ and $\lim_{x\to +\infty}F(x) = 1$. Its derivative is proportional to the probability distribution function. The cumulative distribution function was fitted to that of the two-parameter Weibull distribution $F_{\text{Weibull}}(x) = 1 - \exp\{-(x/b)^c\}$, where b is known as the scaling parameter and c is known as the shape parameter (inset of Figure 2 and Table 1).[43,44] This model is appropriate for the description of the variation in the SSEF, a quantity that is very sensitive to the nanoscale details of the shape of the metal structure, in a system with a large number of degrees of freedom. The structural configuration of a dimer of identical cubes in the context of SERS measurement with linearly polarized light involves 7 degrees of freedom, although in practice 3 of the degrees of freedom are highly constrained by the van der Waals interaction with the substrate. Therefore, we can assume that a very limited set of configurations will produce the optimal SSEF, and a vast number of configurations will lead to SSEFs that are not better than the enhancement observed with a monomer. In the interpretation of the data by the Weibull distribution model, the scaling parameter indicates the *average magnitude* of the enhancement factor that can be achieved and the shape parameter indicates the *sensitivity* of the enhancement factor to deviations from the optimal cluster configuration. The validity of the model was verified against our data sets using the transformation $Y = \ln\{-\ln\{1 - F(x)\}\}$ and $X = \ln\{x\}$, which linearized the data and was used to estimate the values of b and c (Table 1). Coincidentally, Fang *et al.* reported recently that a similar expression and similar parameter values describe the local SERS EF variability in a nanotextured silver film.[45]

The analysis by the Weibull distribution model indicates that the shape parameters of the SSEF distributions for the EE dimers and FE dimers are indistinguishable, but their scale parameters are significantly different. In other words, on average the enhancement factors of FE dimers are a factor of ~2.4 higher than the enhancement factors of EE dimers. This is not to say that the highest SSEF is associated with a dimer of FE type. As seen in Figure 2, thus far, our strongest enhancement was observed in an EE dimer. The reason for this is that the EE dimers are found on our substrate at a higher frequency than the FE dimers, presumably due to an inherent bias in the vertical deposition process. Interestingly, the two groups can be expected to have the same trend in the change of the enhancement factor as the configuration of the dimer deviates from optimum. For example, as we will show later, a similar decay in the SSEF can be expected as a function of gap distance. In contrast, a larger value of the shape parameter was calculated for the distribution of SSEFs of FF dimers. This difference can be seen clearly in the slopes of the fit function $F(x)$ for high values of the enhancement factor in the inset of Figure 2. The very moderate slope in the fit for the FF-type dimers indicates that the portion of strongly enhancing dimers is very small in the FF group. Again, the data could not be used to determine the maximum attainable SSEF for each group. If we considered each measured value individually, we might have been tempted to simplistically rank the maximum SSEF from EE dimers highest and from FF dimers lowest (Figure 2). However, from the analysis of the ensemble of dimers, we determined that this ranking could depend on the number of structures investigated, and a very large number of observations would be necessary to determine it with reasonable confidence. The ranking of the dimer types based on their enhancement factor suggested by Xia *et al.* (FF > FE > EE)[26] is, therefore, not in disagreement with this work, particularly since the two studies were carried out using different excitation wavelengths (see below). The key result of this study is that the azimuthal orientation of nanocubes in the dimer affects the dispersion of enhancement factors observed in a large group of dimers. Since most fabrication techniques cannot reproduce a patterned surface at the atomic scale, SERS substrates are destined to have nanoscale structural variations from site to site, as exhibited by the library of structures used in our study. In the case of a SERS substrate made of AgNC dimers, our study indicates that substrates containing aligned face-to-edge dimers should be considered the most suitable for practical applications, as they display the highest uniformity in their SSEFs and the highest average value of SSEF.

Our experimental research has been complemented by the numerical modeling of plasmon resonance modes and SERS enhancement factors for EE, FE, and FF AgNC dimer configurations, as well as for AgNC monomers. Plasmon modes corresponding to these configurations have been computed (in the electrostatic approximation) through the solution of the eigenvalue problem for specific boundary integral equations.[46,47] As explained in detail in the referenced works, the eigenvalue and the eigenvector solutions are related to the resonance frequency and to the surface charge distribution associated with each localized plasmon mode. Subsequently, steady-state electric field distributions and dipole moments can be calculated as a function of the frequency and intensity of the incident light.[48] The dipolar plasmon modes have been identified because these plasmon modes are most efficiently excited by the incident laser radiation when the dimensions of the

nanoparticles are appreciably smaller than the laser wavelength. The final outcome of these studies is the distributions of electric fields $\mathbf{E}(\boldsymbol{r};w_L)$ and $\mathbf{E}(\boldsymbol{r};w_R)$ from the excitations of the dipole plasmon modes by the incident laser radiation and by the Raman-shifted radiation, respectively. These electric field distributions have been used to compute the enhancement factors. We estimate the *local SERS enhancement* as the product

$$\frac{|\mathbf{E}(\boldsymbol{r};w_L)|^2}{|\mathbf{E}_0(w_L)|^2} \times \frac{|\mathbf{E}(\boldsymbol{r};w_R)|^2}{|\mathbf{E}_0(w_R)|^2} \quad (1)$$

where $|\mathbf{E}_0(w)|^2$ is the intensity of the uniform electric field of frequency w exciting the localized plasmons (considering only the field component parallel to the dipole moment of the plasmon mode) and $|\mathbf{E}(\mathbf{r};w)|^2$ is the intensity of the electric field generated by the dominant plasmon mode at location r as a consequence of the steady-state, uniform field excitation. The parameters w_L and w_R are the frequency of the laser light and of the Raman-shifted light, respectively. In this model, we neglect the fact that the excitation of the plasmons by the Raman-shifted light is not spatially uniform[49] and that the efficiency of coupling between the plasmon excitation and the molecular dipole may be altered by the bonding to the surface of the cube. The SERS EF was calculated by integrating the local SERS enhancement over an open envelope separated by 1 nm from the top five faces of the cubes.

In the simulation of plasmons in dimers (see Figure 3A), the coordinate system is chosen such that the origin is at the center of the gap, in-plane with the bottom face of the AgNCs (the $x-y$ plane), and the dimer axis is parallel to the x axis (*i.e.*, the $x-z$ plane is a mirror-symmetry plane in all cases). The semi-infinite silicon substrate is situated 2 nm below the AgNCs ($\varepsilon = 11.7\varepsilon_0$ for $z < -2$ nm) to account for the presence of a native oxide and the molecules in between the plasmonic structure and the substrate.

An example of the dipole plasmon mode for an FF dimer configuration is presented in Figure 3A. In this figure, the distribution of surface electric charges associated with the dipole mode is shown for 4 nm separation between two 80 nm AgNCs laying 2 nm above a silicon surface. The distribution of the surface electric field replicates the charge distribution. It is clear from Figure 3A that the substrate has a significant effect on the field distribution. The hot-spots are localized not only in the gap between the cubic nanoparticles but also in the gaps between the nanoparticles and the silicon substrate and at the bottom of the outside faces. This is consistent with the *method of images*, which implies that a two-cube system on the substrate is electromagnetically equivalent to the corresponding four-cube system in free space. Our numerical modeling

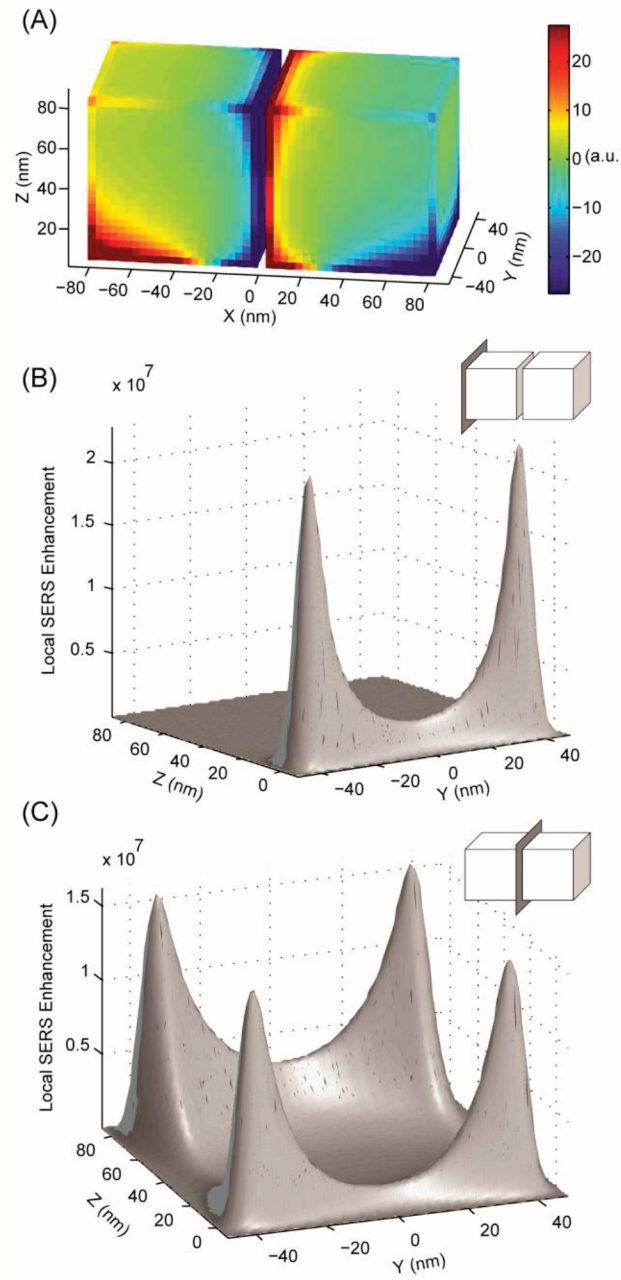

Figure 3. (A) Charge distribution calculated for the dipolar plasmon mode in FF AgNC dimers on a silicon substrate (edge length = 80 nm; gap distance = 4 nm). (B) Local SERS enhancement distribution near the outer faces of the dimer (depicted in the scheme; $x = \pm 83$ nm). (C) Local SERS enhancement distribution near the inner faces of the dimer (depicted in the scheme; $x = \pm 1$ nm). Local SERS enhancement was calculated using eq 1.

demonstrates that the multiple hot-spots occur in FE and EE dimer configurations, as well. These phenomena are consistent with the fact that the total electric charge in each nanoparticle must be equal to zero;[46,47] that is, charges of opposite signs must accumulate in different locations.[20] The calculations are instructive in identifying the size and location of the SERS hot-spots. The SERS EF calculations indicate that contributions of the inner and outer faces to the signal are higher than

TABLE 2. Calculated Resonance Wavelengths and SERS Enhancement Factors for 80 nm Silver Nanocube Dimers on Silicon (Incident Wavelength = 633 nm; Scattered Wavelength = 678 nm)

	FF		FE		EE	
gap distance (nm)	resonance wavelength (nm)	SERS EF	resonance wavelength (nm)	SERS EF	resonance wavelength (nm)	SERS EF
3.0	604.63	6.77×10^6	577.48	1.19×10^6	569.03	6.95×10^5
3.5	595.61	1.63×10^6	573.58	6.87×10^5	567.12	5.01×10^5
4.0	589.08	7.71×10^5	570.52	4.43×10^5	565.35	3.77×10^5
4.5	583.73	4.80×10^5	568.03	3.10×10^5	563.74	2.96×10^5
5.0	578.43	3.49×10^5	565.95	2.32×10^5	562.27	2.40×10^5
5.5	573.13	2.75×10^5	564.19	1.82×10^5	560.95	2.00×10^5
6.0	567.78	2.18×10^5	562.67	1.49×10^5	559.74	1.71×10^5
6.5	562.18	1.59×10^5	561.34	1.26×10^5	558.64	1.48×10^5
7.0	556.32	1.02×10^5	560.17	1.09×10^5	557.63	1.31×10^5
7.5	550.38	5.82×10^4	559.12	9.62×10^4	556.71	1.18×10^5
8.0	544.74	3.21×10^4	558.17	8.64×10^4	555.87	1.07×10^5
8.5	539.46	1.79×10^4	557.32	7.85×10^4	555.08	9.78×10^4
9.0	534.54	1.04×10^4	556.53	7.22×10^4	554.36	9.04×10^4
9.5	530.00	6.19×10^3	555.82	6.70×10^4	553.69	8.42×10^4
10.0	525.79	4.07×10^3	555.16	6.27×10^4	553.07	7.89×10^4

those of the side and top faces. Figure 3B shows the distribution of local SERS enhancement in the above-mentioned FF dimer near the faces of the cubes farthest away from the gap (*i.e.*, the outer faces). The enhancement is highly localized at the bottom of the face, illustrating the strong influence of the substrate on the plasmon mode. Figure 3C shows the corresponding distribution near the faces forming the 4 nm gap (*i.e.*, the inner faces). The enhancement near the four corners is approximately the same, and notably, the enhancement is not very localized. A significant fraction of the molecules adsorbed on the inner faces experiences electric fields of strengths approaching that of the field near the corners. In this FF-type gap, the hot-spot is diffuse and extends over all but a circular area in the center of the faces.

The calculated SERS EF for a single 80 nm AgNC (monomer) with $\lambda_L = c/w_L = 633$ nm and $\lambda_R = c/w_R = 678$ nm is 1.78×10^4, and for a single 100 nm AgNC with $\lambda_L = 514$ nm and $\lambda_R = 560$ nm is 2.14×10^6. The dipole plasmon mode of the monomer was calculated as having a resonance wavelength of 533 nm and a dipole oriented along the diagonal of the bottom/top face. The calculated EFs are commensurate with experimental results[31] and point to a match between the plasmon resonance frequency of an individual AgNC and the frequency of the argon ion laser light (see below).

Table 2 summarizes the results of our computations by presenting the resonance wavelengths and the SERS enhancement factors computed for various gap distances between AgNCs in the cases of FF, FE, and EE dimer configurations. It is apparent that the computational results are quantitatively consistent with the experimental results shown in Figure 2. The most prominent trend seen in Table 2 is that the SERS enhancement factor is more sensitive to the separation between the nanocubes in the FF configuration than in the FE and EE configurations. As the gap increases from 3 to 10 nm, the calculated resonance wavelength shifts from 605 to 526 nm in the FF configuration (away from the laser wavelength), whereas it only changes by 22 and 16 nm in the FE and EE configurations, respectively. The matching condition between the incident wavelength, the scattered wavelength, and the plasmon resonance wavelength[50−52] is therefore difficult to guarantee in FF dimers without precise control over the gap distance in the order of 1 nm or less. The calculated SERS EFs for FF configurations vary by a factor of 1600 with varying gap distance. The variation in the calculated EFs in the FE and EE configurations is only by a factor of 10 to 20. This numerical observation is supported by the cumulative fraction *versus* enhancement factor graphs shown in Figure 2. The dispersion in enhancement factors in the experiment is obviously larger that the calculated ones because in the experiment parameters other than the gap distance (markedly, the orientation of the dimer axis

TABLE 3. Calculated Resonance Wavelengths and SERS Enhancement Factors for 100 nm Silver Nanocube Face-to-Face Dimers on Silicon (Incident Wavelength = 514 nm; Scattered Wavelength = 560 nm)

gap distance (nm)	resonance wavelength (nm)	SERS EF
5	589.08	5.18×10^5
5.625	583.73	8.22×10^5
6.25	578.43	1.48×10^6
6.875	573.13	3.10×10^6
7.5	567.78	7.59×10^6
8.125	562.18	1.80×10^7
8.75	556.32	1.58×10^7
9.375	550.38	6.50×10^6
10	544.74	2.98×10^6

with respect to the light polarization) contribute to site-to-site variations. We have also compared our simulation results with the experimental results from Xia *et al.*,[26] where similar dimer configurations have been studied for incident laser radiation wavelength of 514.5 nm and a Raman-shifted radiation wavelength of 560 nm. The results of our computations are shown in Table 3 for the FF configuration, and they are consistent with the experimental observation from the referenced work[26] where a Raman enhancement factor of 2.0×10^7 was obtained. Table 3 illustrates also the dependence of SERS EF on both the resonance condition and the surface structure. As the gap distance increases, the field is more uniformly distributed over the surface of the cubes (less localized in the gap) but simultaneously the plasmon resonance shifts to higher frequencies and closer to the incident and scattered radiation frequencies. These two opposing effects lead to an increase and then to a decrease in the EF as the gap is varied. This non-monotonic response can be seen only with the proper choice of laser energy.

In the in-depth numerical studies described above, the dimer structures were of high degree of symmetry: the FF, FE, and EE dimers modeled belong to the point groups D_{4h}, C_{2v}, and D_{2h}, respectively, when the silicon substrate is excluded. Preliminary investigations with reduced-symmetry dimers obtained by shifting one of the AgNCs in the *y*-direction perpendicular to the dimer axis demonstrated that the numerical results are not strongly dependent on the symmetry; that is, the system is largely insensitive to such perturbations in the positioning of the cubes.

Our simulations also show that another dipole resonant plasmon mode may appear in the same wavelength range as the separation between the cubic nanoparticles is increased. This is consistent with the experimental report by Van Duyne *et al.*[53] on the extinction cross section of a single cubic nanoparticle placed on a glass substrate. Two closely spaced peaks in the extinction cross section were reported, which clearly correspond to the excitations of two distinct plasmon modes. It will be beneficial for SERS enhancement to tune the laser wavelength in such a way that near resonance excitations of these two plasmon modes are simultaneously achieved by the laser radiation and the Raman-shifted radiation, respectively.[54]

For comparison, the case of AgNC monomers will be briefly discussed here. Individual AgNCs provide less surface area for molecular absorption and lower average field enhancement in comparison to dimers and, therefore, weaker SERS signals. Under excitation with a 632.8 nm laser, the SERS signals were close to or below our detection limit, corresponding to SSEFs of no more than 2×10^4. With a high intensity Ar ion laser operating at 514.5 nm, the detection threshold was lower, the enhancements were expected to be higher, and indeed, signal was routinely recorded from individual AgNCs. The SSEFs recorded were up to $\sim 1 \times 10^5$ using the 1078 cm^{-1} peak for the estimation of the EF value (higher values could be obtained with the 1562 cm^{-1} peak). Enhancement factors of up to 3×10^6 were reported previously using the excitation wavelength of 514.5 nm with AgNC monomers.[23,31,55] Discrepancies in reported values between researchers can be attributed to different ways the EFs are calculated and uncertainty in determining the number of molecules in the excitation volume of the laser beam, the resonance conditions of the system, and contributions from the *chemical mechanism* of enhancement. Regardless, the presence of a second cube (as in the dimer) leads to the augmentation of the SERS enhancement. However, this augmentation is much more significant under the experimental conditions that were chosen in this work, up to almost 3 orders of magnitude, compared with a factor of ~ 10 when an Ar ion laser is used. We reason that this is due to the fact that the 632.8 nm laser light is far from the plasmon resonances of the AgNC monomer but may be close to resonance with regard to a dipole plasmon mode of the dimer. Furthermore, we have chosen to study a vibration mode that is very strong in the normal Raman spectrum of the molecule, and therefore, it is probably less susceptible to chemical enhancement. The studies with 514.5 nm laser light are near resonance with the AgNC monomer, allowing for signal detection from a single cube but diminishing the significance of the coupling in the dimer. Thus, when preparing substrates for SERS equipment based on 514.5 nm light source, it may be less advantageous to use dimers since complications arising from the dispersion in enhancement may overshadow the gain in enhancement.

CONCLUSION

In this paper, we explored for the first time the dispersion of enhancement factors in a SERS substrate made through self-assembly of silver nanocubes. This analysis was possible thanks to the control over the locations on the substrate in which clusters of nanocubes were formed, which was achieved by trapping the nanoparticles in cavities in prepatterned substrates. This approach allowed for the acquisition of Raman spectra and microscopy images of individual AgNC dimers without bias. Correlations between SERS signal intensity and SERS substrate enhancement factor and various structural parameters of the dimers were established. In particular, the dispersion of SSEF values was found to be significantly greater in face-to-face dimers than in face-to-edge and edge-to-edge dimers. Numerical calculations of plasmon resonance frequencies and enhancement factors provided further support for the

correlations that were established experimentally. These data support the notion that proper plasmon resonance wavelength tuning with respect to the laser wavelength can be beneficial to SERS enhancement. Furthermore, some plasmonic structures for SERS substrates require more precise fabrication tools than others because they show a higher dispersion in the enhancement factor.

METHODS

Materials. AgNCs were synthesized following a previously reported protocol.[56,57] 1,5-Pentanediol (Acros, 98%), silver nitrate (Alfa-Aesar, 99.995% metal base), copper(II) chloride (Sigma-Aldrich, 97%), polyvinylpyrrolidone (Sigma-Aldrich, M_w = 55K), and 4-aminobenzenethiol (Sigma-Aldrich, 97%) were used as received. Polymethylmethacrylate e-beam resist (950PMMA A4) and developer (MIBK/IPA 1:3 developer) were purchased from MicroChem Corp.

Preparation of SERS Substrates. Square arrays of 200 nm diameter pores were formed by conventional e-beam lithography. PMMA e-beam resist was spin-coated on a silicon wafer to a thickness of 200 nm and subsequently baked at 180 °C for 1 min. The electron beam lithography was carried out using a Raith e_LiNE system with an accelerating voltage of 15 keV and an exposure dose of 140 μC/cm^2 using a 10 μm aperture. After writing and developing, the patterns in the PMMA film were transferred to the underlying silicon substrate by dry etch. The dry etch was carried out in a reactive ion etching system (Trion Tech.) using a SF_6/O_2 gas mixture (50:10 sccm) at a power of 100 W for 10 s. The etch depth was 90−100 nm. The residual of PMMA was removed by acetone rinse and O_2 plasma clean (50 W, 5 min). The patterned substrate was immersed vertically in a suspension of AgNCs in water and slowly pulled out by means of a motorized stage at the speed of 0.3 mm/h. Excess AgNCs on the surface were removed by gentle brushing. The substrate was then immersed in a 0.2 mM 4-ABT solution in ethanol for 3 h, rinsed extensively with ethanol, and dried under nitrogen.

Characterization of the AgNC Clusters. SERS spectra were measured with a Horiba Jobin-Yvon LabRAM HR-VIS micro-Raman spectrometer equipped with a 632.8 nm laser source, a confocal microscope, and an $x-y$ scanning stage. A 50× objective (numerical aperture NA = 0.5) was used for signal collection. SERS spectra were acquired with incident laser power of 0.6 mW and acquisition time of 4 s. Images of the pores were recorded by SEM (Hitachi, SU-70) immediately after the Raman measurement.

Raman Spectra Analysis and Calculation of the SERS Substrate Enhancement Factor. The Raman signal intensity is quantified as the integrated peak area for the carbon−sulfur bond stretch of 4-ABT at 1078 cm^{-1} in each spectrum. Using the same spectrometer settings, a reference Raman spectrum of a 1.0 M solution of 4-ABT in 1,5-pentanediol was measured, and the Raman signal intensity per molecule was calculated assuming a cylindrical focal volume of ϕ2.2 μm × 16 μm. The SERS substrate enhancement factor (SSEF) is calculated as the Raman signal intensity divided by the number of molecules on the AgNCs and by the Raman signal intensity per molecule (from the reference spectrum). A monolayer of 4-ABT molecules on the six {001} facets of the AgNCs is considered, with a density of 5 molecules/nm^2.[58]

Numerical Simulations. Plasmon resonance frequencies and the surface charge distributions associated with each localized plasmon mode were computed by solving the eigenvalue problem for specific boundary integral equations, as published previously.[46,47] These integral equations were discretized by partitioning the surface of each cube into triangular patches and were solved using LAPACK (version 3.0) eigenvalue solvers. The computations were repeated with 19 200 and 30 000 triangular patches for each cube and produced practically the same results. Steady-state electric field distributions were calculated as a function of the frequency and intensity of the incident light using analytical formulas presented in ref 48. There are many approaches to modeling the plasmonic response of nanostructures, each with advantages and disadvantages with respect to computational cost, generality, and accuracy. The main advantage of the eigenvalue method for plasmon mode analysis is that it provides insight into the symmetry and nature of the optical interactions. Additionally, since the method separates the effect of sample geometry and sample dispersion relation, in a single computation we solve for any material (gold, silver, *etc.*) and for any laser polarization. With FDTD methods, any change in the materials system or in the orientation of the laser field requires a new computation.

The numerical simulations were performed for ideal geometries of EE, FE, and FF AgNC dimer configurations, as well as for AgNC monomers. The nanocube edge length was 80 or 100 nm. The complex permittivity of silver was obtained from the literature.[59] The dielectric constant of silicon substrate was set to 11.7ε_0.

Acknowledgment. This work was supported in part by DBED State of Maryland, as well as by ONR and NSF. We appreciate the support of the Maryland NanoCenter and its NispLab. The NispLab is supported in part by the NSF as a MRSEC Shared Experimental Facility.

Supporting Information Available: Data on the dependence of the SERS signal on laser polarization. Procedure for assigning the dimer type as EE, FE, or FF based on geometrical factors. This material is available free of charge *via* the Internet at http://pubs.acs.org.

REFERENCES AND NOTES

1. Camden, J. P.; Dieringer, J. A.; Zhao, J.; Van Duyne, R. P. Controlled Plasmonic Nanostructures for Surface-Enhanced Spectroscopy and Sensing. *Acc. Chem. Res.* **2008**, *41*, 1653–1661.
2. Kneipp, K.; Kneipp, H.; Itzkan, I.; Dasari, R. R.; Feld, M. S. Surface-Enhanced Raman Scattering and Biophysics. *J. Phys.: Condens. Matter* **2002**, *14*, R597–R624.
3. Moskovits, M. Surface-Enhanced Raman Spectroscopy: A Brief Retrospective. *J. Raman Spectrosc.* **2005**, *36*, 485–496.
4. Kneipp, K.; Wang, Y.; Kneipp, H.; Perelman, L. T.; Itzkan, I.; Dasari, R. R.; Feld, M. S. Single Molecule Detection Using Surface-Enhanced Raman Scattering (SERS). *Phys. Rev. Lett.* **1997**, *78*, 1667–1670.
5. Nie, S.; Emory, S. R. Probing Single Molecules and Single Nanoparticles by Surface-Enhanced Raman Scattering. *Science* **1997**, *275*, 1102–1106.
6. Xu, H. X.; Bjerneld, E. J.; Kall, M.; Borjesson, L. Spectroscopy of Single Hemoglobin Molecules by Surface Enhanced Raman Scattering. *Phys. Rev. Lett.* **1999**, *83*, 4357–4360.
7. Weiss, A.; Haran, G. Time-Dependent Single-Molecule Raman Scattering as a Probe of Surface Dynamics. *J. Phys. Chem. B* **2001**, *105*, 12348–12354.
8. Camden, J. P.; Dieringer, J. A.; Wang, Y. M.; Masiello, D. J.; Marks, L. D.; Schatz, G. C.; Van Duyne, R. P. Probing the Structure of Single-Molecule Surface-Enhanced Raman Scattering Hot Spots. *J. Am. Chem. Soc.* **2008**, *130*, 12616–12617.
9. Dieringer, J. A.; Lettan, R. B.; Scheidt, K. A.; Van Duyne, R. P. A Frequency Domain Existence Proof of Single-Molecule Surface-Enhanced Raman Spectroscopy. *J. Am. Chem. Soc.* **2007**, *129*, 16249–16256.
10. Blackie, E.; Le Ru, E. C.; Meyer, M.; Timmer, M.; Burkett, B.; Northcote, P.; Etchegoin, P. G. Bi-Analyte SERS with Isotopically Edited Dyes. *Phys. Chem. Chem. Phys.* **2008**, *10*, 4147–4153.
11. Brown, R. J. C.; Milton, M. J. T. Nanostructures and Nanostructured Substrates for Surface-Enhanced Raman Scattering (SERS). *J. Raman Spectrosc.* **2008**, *39*, 1313–1326.

12. Creighton, J. A.; Blatchford, C. G.; Albrecht, M. G. Plasma Resonance Enhancement of Raman-Scattering by Pyridine Adsorbed on Silver or Gold Sol Particles of Size Comparable to the Excitation Wavelength. *J. Chem. Soc., Faraday Trans. 2* **1979**, *75*, 790–798.
13. Michaels, A. M.; Jiang, J.; Brus, L. Ag Nanocrystal Junctions as the Site for Surface-Enhanced Raman Scattering of Single Rhodamine 6G Molecules. *J. Phys. Chem. B* **2000**, *104*, 11965–11971.
14. Rodriguez-Lorenzo, L.; Alvarez-Puebla, R. A.; Pastoriza-Santos, I.; Mazzucco, S.; Stephan, O.; Kociak, M.; Liz-Marzan, L. M.; de Abajo, F. J. G. Zeptomol Detection through Controlled Ultrasensitive Surface-Enhanced Raman Scattering. *J. Am. Chem. Soc.* **2009**, *131*, 4616–4618.
15. Gunnarsson, L.; Bjerneld, E. J.; Xu, H.; Petronis, S.; Kasemo, B.; Kall, M. Interparticle Coupling Effects in Nanofabricated Substrates for Surface-Enhanced Raman Scattering. *Appl. Phys. Lett.* **2001**, *78*, 802–804.
16. Mulvihill, M.; Tao, A.; Benjauthrit, K.; Arnold, J.; Yang, P. Surface-Enhanced Raman Spectroscopy for Trace Arsenic Detection in Contaminated Water. *Angew. Chem., Int. Ed.* **2008**, *47*, 6456–6460.
17. Li, W.; Camargo, P. H. C.; Au, L.; Zhang, Q.; Rycenga, M.; Xia, Y. Etching and Dimerization: A Simple and Versatile Route to Dimers of Silver Nanospheres with a Range of Sizes. *Angew. Chem., Int. Ed.* **2010**, *49*, 164–168.
18. Talley, C. E.; Jackson, J. B.; Oubre, C.; Grady, N. K.; Hollars, C. W.; Lane, S. M.; Huser, T. R.; Nordlander, P.; Halas, N. J. Surface-Enhanced Raman Scattering from Individual Au Nanoparticles and Nanoparticle Dimer Substrates. *Nano Lett.* **2005**, *5*, 1569–1574.
19. Camargo, P. H. C.; Rycenga, M.; Au, L.; Xia, Y. Isolating and Probing the Hot Spot Formed between Two Silver Nanocubes. *Angew. Chem., Int. Ed.* **2009**, *48*, 2180–2184.
20. Kim, D.-S.; Heo, J.; Ahn, S.-H.; Han, S. W.; Yun, W. S.; Kim, Z. H. Real-Space Mapping of the Strongly Coupled Plasmons of Nanoparticle Dimers. *Nano Lett.* **2009**, *9*, 3619–3625.
21. Yang, S. C.; Kobori, H.; He, C. L.; Lin, M. H.; Chen, H. Y.; Li, C. C.; Kanehara, M.; Teranishi, T.; Gwo, S. Plasmon Hybridization in Individual Gold Nanocrystal Dimers: Direct Observation of Bright and Dark Modes. *Nano Lett.* **2010**, *10*, 632–637.
22. Wei, H.; Hao, F.; Huang, Y. Z.; Wang, W. Z.; Nordlander, P.; Xu, H. X. Polarization Dependence of Surface-Enhanced Raman Scattering in Gold Nanoparticle−Nanowire Systems. *Nano Lett.* **2008**, *8*, 2497–2502.
23. Camargo, P. H. C.; Cobley, C. M.; Rycenga, M.; Xia, Y. Measuring the Surface-Enhanced Raman Scattering Enhancement Factors of Hot Spots Formed between an Individual Ag Nanowire and a Single Ag Nanocube. *Nanotechnology* **2009**, *20*, 434020.
24. McLellan, J. M.; Li, Z. Y.; Siekkinen, A. R.; Xia, Y. The SERS Activity of a Supported Ag Nanocube Strongly Depends on Its Orientation Relative to Laser Polarization. *Nano Lett.* **2007**, *7*, 1013–1017.
25. Natan, M. J. Concluding Remarks—Surface Enhanced Raman Scattering. *Faraday Discuss.* **2006**, *132*, 321–328.
26. Camargo, P. H. C.; Au, L.; Rycenga, M.; Li, W. Y.; Xia, Y. Measuring the SERS Enhancement Factors of Dimers with Different Structures Constructed from Silver Nanocubes. *Chem. Phys. Lett.* **2010**, *484*, 304–308.
27. Liddle, J. A.; Cui, Y.; Alivisatos, P. Lithographically Directed Self-Assembly of Nanostructures. *J. Vac. Sci. Technol., B* **2004**, *22*, 3409–3414.
28. Alexander, K. D.; Hampton, M. J.; Zhang, S.; Dhawan, A.; Xu, H.; Lopez, R. A High-Throughput Method for Controlled Hot-Spot Fabrication in SERS-Active Gold Nanoparticle Dimer Arrays. *J. Raman Spectrosc.* **2009**, *40*, 2171–2175.
29. Rycenga, M.; Camargo, P. H. C.; Xia, Y. Template-Assisted Self-Assembly: A Versatile Approach to Complex Micro- and Nanostructures. *Soft Matter* **2009**, *5*, 1129–1136.
30. Yan, B.; Thubagere, A.; Premasiri, W. R.; Ziegler, L. D.; Dal Negro, L.; Reinhard, B. M. Engineered SERS Substrates with Multiscale Signal Enhancement: Nanoparticle Cluster Arrays. *ACS Nano* **2009**, *3*, 1190–1202.
31. Rycenga, M.; Kim, M. H.; Camargo, P. H. C.; Cobley, C.; Li, Z. Y.; Xia, Y. Surface-Enhanced Raman Scattering: Comparison of Three Different Molecules on Single-Crystal Nanocubes and Nanospheres of Silver. *J. Phys. Chem. A* **2009**, *113*, 3932–3939.
32. Le Ru, E. C.; Blackie, E.; Meyer, M.; Etchegoin, P. G. Surface Enhanced Raman Scattering Enhancement Factors: A Comprehensive Study. *J. Phys. Chem. C* **2007**, *111*, 13794–13803.
33. Xu, H. X.; Aizpurua, J.; Kall, M.; Apell, P. Electromagnetic Contributions to Single-Molecule Sensitivity in Surface-Enhanced Raman Scattering. *Phys. Rev. E* **2000**, *62*, 4318–4324.
34. Jiang, J.; Bosnick, K.; Maillard, M.; Brus, L. Single Molecule Raman Spectroscopy at the Junctions of Large Ag Nanocrystals. *J. Phys. Chem. B* **2003**, *107*, 9964–9972.
35. Etchegoin, P. G.; Galloway, C.; Le Ru, E. C. Polarization-Dependent Effects in Surface-Enhanced Raman Scattering (SERS). *Phys. Chem. Chem. Phys.* **2006**, *8*, 2624–2628.
36. Du, C. L.; Yang, M. X.; You, Y. M.; Chen, T.; Chen, H. Y.; Shen, Z. X. Polymer-Encapsulated Silver Nanoparticle Monomer and Dimer for Surface-Enhanced Raman Scattering. *Chem. Phys. Lett.* **2009**, *473*, 317–320.
37. Li, W.; Camargo, P. H. C.; Lu, X.; Xia, Y. Dimers of Silver Nanospheres: Facile Synthesis and Their Use as Hot Spots for Surface-Enhanced Raman Scattering. *Nano Lett.* **2009**, *9*, 485–490.
38. Xu, H. X.; Kall, M. Polarization-Dependent Surface-Enhanced Raman Spectroscopy of Isolated Silver Nanoaggregates. *ChemPhysChem* **2003**, *4*, 1001–1005.
39. Sundaramurthy, A.; Crozier, K. B.; Kino, G. S.; Fromm, D. P.; Schuck, P. J.; Moerner, W. E. Field Enhancement and Gap-Dependent Resonance in a System of Two Opposing Tip-to-Tip Au Nanotriangles. *Phys. Rev. B* **2005**, *72*, 165409.
40. Schuck, P. J.; Fromm, D. P.; Sundaramurthy, A.; Kino, G. S.; Moerner, W. E. Improving the Mismatch between Light and Nanoscale Objects with Gold Bowtie Nanoantennas. *Phys. Rev. Lett.* **2005**, *94*, 017402.
41. Qin, L.; Zou, S.; Xue, C.; Atkinson, A.; Schatz, G. C.; Mirkin, C. A. Designing, Fabricating, and Imaging Raman Hot Spots. *Proc. Natl. Acad. Sci. U.S.A.* **2006**, *103*, 13300–13303.
42. When the geometry of the dimer was intermediate with respect to unambiguous EE, FE, and FF structures, the criteria outlined in the Supporting Information were used to make consistent assignments to the groups.
43. Murthy, D. N. P.; Xie, M.; Jiang, R. *Weibull Models*; John Wiley & Sons, Inc.: Hoboken, NJ, 2004.
44. Rinne, H. *The Weibull Distribution: A Handbook*; CRC Press: Boca Raton, FL, 2008.
45. Fang, Y.; Seong, N. H.; Dlott, D. D. Measurement of the Distribution of Site Enhancements in Surface-Enhanced Raman Scattering. *Science* **2008**, *321*, 388–392.
46. Fredkin, D. R.; Mayergoyz, I. D. Resonant Behavior of Dielectric Objects (Electrostatic Resonances). *Phys. Rev. Lett.* **2003**, *91*, 253902.
47. Mayergoyz, I. D.; Fredkin, D. R.; Zhang, Z. Y. Electrostatic (Plasmon) Resonances in Nanoparticles. *Phys. Rev. B* **2005**, *72*, 155412.
48. Mayergoyz, I. D.; Zhang, Z.; Miano, G. Analysis of Dynamics of Excitation and Dephasing of Plasmon Resonance Modes in Nanoparticles. *Phys. Rev. Lett.* **2007**, *98*, 147401.
49. Davis, T. J.; Gómez, D. E.; Vernon, K. C. Interaction of Molecules with Localized Surface Plasmons in Metallic Nanoparticles. *Phys. Rev. B* **2010**, *81*, 045432.
50. Haynes, C. L.; Van Duyne, R. P. Plasmon-Sampled Surface-Enhanced Raman Excitation Spectroscopy. *J. Phys. Chem. B* **2003**, *107*, 7426–7433.
51. McFarland, A. D.; Young, M. A.; Dieringer, J. A.; Van Duyne, R. P. Wavelength-Scanned Surface-Enhanced Raman Excitation Spectroscopy. *J. Phys. Chem. B* **2005**, *109*, 11279–11285.
52. Dadosh, T.; Sperling, J.; Bryant, G. W.; Breslow, R.; Shegai,

T.; Dyshel, M.; Haran, G.; Bar-Joseph, I. Plasmonic Control of the Shape of the Raman Spectrum of a Single Molecule in a Silver Nanoparticle Dimer. *ACS Nano* **2009**, *3*, 1988–1994.
53. Sherry, L. J.; Chang, S. H.; Schatz, G. C.; Van Duyne, R. P.; Wiley, B. J.; Xia, Y. Localized Surface Plasmon Resonance Spectroscopy of Single Silver Nanocubes. *Nano Lett.* **2005**, *5*, 2034–2038.
54. Chu, Y. Z.; Banaee, M. G.; Crozier, K. B. Double-Resonance Plasmon Substrates for Surface-Enhanced Raman Scattering with Enhancement at Excitation and Stokes Frequencies. *ACS Nano* **2010**, *4*, 2804–2810.
55. Rycenga, M.; Camargo, P. H. C.; Li, W.; Moran, C. H.; Xia, Y. Understanding the SERS Effects of Single Silver Nanoparticles and Their Dimers, One at a Time. *J. Phys. Chem. Lett.* **2010**, *1*, 696–703.
56. Tao, A.; Sinsermsuksakul, P.; Yang, P. D. Polyhedral Silver Nanocrystals with Distinct Scattering Signatures. *Angew. Chem., Int. Ed.* **2006**, *45*, 4597–4601.
57. Tao, A. R.; Ceperley, D. P.; Sinsermsuksakul, P.; Neureuther, A. R.; Yang, P. D. Self-Organized Silver Nanoparticles for Three-Dimensional Plasmonic Crystals. *Nano Lett.* **2008**, *8*, 4033–4038.
58. Gole, A.; Sainkar, S. R.; Sastry, M. Electrostatically Controlled Organization of Carboxylic Acid Derivatized Colloidal Silver Particles on Amine-Terminated Self-Assembled Monolayers. *Chem. Mater.* **2000**, *12*, 1234–1239.
59. Johnson, P. B.; Christy, R. W. Optical-Constants of Noble-Metals. *Phys. Rev. B* **1972**, *6*, 4370–4379.